Asian Journal of Chemistry; Vol. 34, No. 7 (2022), 1665-1674

ASIAN JOURNAL OF CHEMISTRY

https://doi.org/10.14233/ajchem.2022.23622

DFT Calculations of 2,5-Diphenyl Furan against SARS-CoV-2 M^{pro} based on Molecular Docking Approach

S. JEYAVIJAYAN[1,*], M. RAMUTHAI[1] and PALANI MURUGAN[2]

[1]Department of Physics, Kalasalingam Academy of Research and Education, Krishnankoil-626126, India
[2]Department of Physics, Dr. B.R. Ambedkar Institute of Technology, Port Blair-744103, Andaman & Nicobar Islands, India

*Corresponding author: E-mail: sjeyavijayan@gmail.com

Received: 15 November 2021; *Accepted*: 2 February 2022; *Published online*: 15 June 2022; AJC-20838

FTIR, FT-Raman and density functional theory (DFT) studies of 2,5-diphenyl furan (DPF) has been carried out to interpret the molecular structure, vibrational frequencies and its intensities. From the estimation, we obtained the HOMO-LUMO energy gap as 2.7113 eV, which is clearly significant the charge transfer occurs within the molecule. The intramolecular interaction and delocalization of the charges has been studied using NBO analysis. In addition, molecular electrostatic potential (MEP) calculations were also performed. The hydrogen bond interactions and binding energy of 2,5-diphenyl furan were estimated using molecular docking studies. The docking investigation was carried out to confirm the repressive nature of title molecule against SARS-CoV-2 main protease (M^{pro}) proteins.

Keywords: Density functional theory, 2,5-Diphenyl furan, SARS-CoV-2 M^{pro}, Molecular docking.

INTRODUCTION

Coronaviridae is a family of enveloped, positive-strand RNA virus, which infects mainly amphibians birds and mammals. Some of the variants of coronaviridae such as severe acute syndrome coronavirus (SARS-CoV), middle east respiratory syndrome coronavirus (MERS-CoV) are notable variants which are induced from animals to humans. These respiratory syndromes cause many deaths in past decades. The intermediate transmission host from bat to human still found unknown and still human to human transmission need to be validated [1]. Unlike other RNA viruses, the SARS-CoV-2 has longest genome sequence that ranging from 26 to 32 kb in length, which contains more than 20 proteins some of those are namely main protease (M^{pro}), 3-chymotrypsin-like protease (3CL^{pro}). 3CL^{pro} of novel corona virus or SARS-CoV-2 is identical about 96.1% and homodimeric cysteine protease of M^{pro} plays vital role during replication and transmission of SARS virus. The M^{pro} driven enzyme downstream and cleaves the remaining 11 non-structural proteins of polyproteins into polypeptides. These polypeptides associate with the replication process of the virus. Hence, the M^{pro} of SARS-CoV-2 is targeted for the drug development [2]. The M^{pro} of SARS-CoV-2 progressively inhibit by 2,5-diphenyl furan (DPF) which is practiced for clinical trial for treating COVID-19 diagnosing. Adopting Computer Aided Drug Design (CADD) system to develop a new drug decreases the time span and cost for drug development and to determine the most critical ligand binding energy factor [3].

Furan is typical aromatic heterocyclic compound and found in natural plants, many processed foods, beverages counterfeit medicines with highly stable chemical structure. The main source of furan have been obtained from the thermally degradation of amino acids and carbohydrates. Recent studies on furan and its derivatives pose many antivirals, antifungal, anti-bacterial, antitumorigenic, anti-inflammatory, antifertility, hypoglycemic and cytostatic properties [4-6]. The day-by-day advancement on heterocyclic chemistry leads to deep interest to the researchers to develop new drugs. From the literature report, no computation study has been done on 2,5-diphenyl furan (DPF) molecule as a powerful drug application [7-9]. In DFT approaches, Becke's three-parameter hybrid function associated with the Lee-Yang-Parr relationship (B3LYP) expects good calculation for infrared, vibrational wavenumbers, molecular geometries and molecular orbital energies [10,11]. In this study, the structural and electronic excited states related to stability and reactivity of DPF has been computed

with DFT/B3LYP technique. The present work has also been focused to identify the Mullikan charges and natural bond orbitals (NBO) of DPF. From the Molecular docking analysis [12], the binding scores of the receptors are found more efficient against SARS-CoV-2 M^{pro}, which provide pathway to enhancement in clinical diagnoses.

EXPERIMENTAL

Pure 2,5-diphenyl furan (DPF) have been obtained from Sigma-Aldrich, USA. The vibration frequencies were recorded with the help of Perkin Elmer Fourier Transform Infrared (FTIR) spectrometer at room temperature with 1 cm^{-1} resolution in the wavenumber ranges from 4000 to 400 cm^{-1}. using KBr and DPF mixed uniformly to obtain the pellet with the assist of pelletizer. The Bruker RFS 27 FT-Raman Spectrometer with resolution of 2 cm^{-1} have been used to study standalone sample of DPF at room temperature with the wavenumber ranges from 4000 cm^{-1} to 50 cm^{-1}.

Computational methods: The GAUSSIAN 09W program [13] has been exploited for DFT calculations. Initially, the structure of 2,5-diphenyl furan (DPF) was optimized by the DFT/B3LYP [14,15] approach with larger basis set 6-311++G (d,p) and then the frequency wavenumbers, intensities are calculated. The scaled quantum mechanical (SQM) [16] method have been used to compare the experimental data and DFT results. Hence, the computed vibrations were scaled by employing a scaling value of 0.9613 for the B3LYP method [17]. The frontier molecular orbitals (FMOs) of DPF have been visualized by Gaussview 05 visualization program [18]. The UV-Vis region of DPF have been calculated (without any solvation) by using time-dependent (TD)-DFT/B3LYP method. The ^{13}C & ^{1}H NMR shielding have been recorded using the Gauge-Invariant-atomic orbital (GIAO) method. The vibrational wavenumbers of each functional group of DPF have been confirmed from the total energy distribution (TED) using MOLVIB program [19].

Molecular docking: The ligand binding response and affinity of SARS-CoV-2 M^{pro} is identified rapidly by employing the Autodock Vina (Version: 4.2.1) [20] package. The PDBQT file has been generated with the complex parameters using Autodock soft tools. Gasteiger-Marsili approach was used to predict the atomic charges of ligands and receptor bonding and the lowest binding energy results the best docking mode. The grid size has been selected as 26 × 26 × 26 Å. The grid center has been selected as the center of mass of aza-peptide epoxide, which is bound to the active site of SARS-CoV-2 M^{pro}.

Protein and ligand structure: In the docking study, the interaction between DPF with the of SARS-CoV-2 M^{pro} marker protein have been analyzed. The title molecule, DPF have been used as a ligand and the crystal structure of protein marker including of SARS-CoV-2 M^{pro} [PDB ID: 7JMO] were used as the targeted protein. This protein data was extracted from the site (http://www.pdb.org) [21] and a ligand DPF and its structure have been gotten from the open ligand databases: PubChem (http://pubchem.ncbi.nlm.nih.gov). The ligand and targeted proteins were prepared using MGL Tools 1.5.4. To expect the ligand conformation in the active site of the targeted proteins, the results were evaluated for all calculation to get the affinity energies, considering the RMSD between original and subsequent structures. In addition, the Discovery Studio (Version: R2 2017 client) [22] software have been used to estimate the amino acid position and protein structure, trailed by the molecular docking with DPF. Discovery Studio was also used to form the non-covalent interactions for all complexes, the number of hydrogen bonds and to make the figures for the complexes with interaction maps.

RESULTS AND DISCUSSION

Molecular structure analysis: The optimized structure of 2,5-diphenyl furan (DPF) having C_1 point group is shown in Fig. 1. By using the B3LYP method with 6-311++G (d,p) premise set, the computed optimized parameters of DPF along with XRD [23] data are recorded in Table-1. From the computational results, most of the bond distances are slightly bigger than the experimental values, due to that the DFT calculations carried out in gaseous stage whereas the observed results carried out in different state. The global least energy obtained for DPF is calculated as -692.32434811 Hartrees. The C-H bond would be affected by the impacts of the inductive-mesomeric interactions [24]. The C-H bond length changes from 1.0857 to 1.0998 Å. The C-C bond distances extend from 1.3796 to 1.540 Å by the B3LYP/6-311G++ (d,p) strategy, which are good assertion with those experimental XRD (1.3750-1.5262 Å) report. The structure of DPF is slightly out of hexagonal due to the diphenyl and furan groups. From the DFT calculations, the C2-O1-C5, O1-C2-C19 and C5-C4-H7 bond angles are computed as 106.56º, 114.45º and 127.76º, respectively, (Experimental values: 107.52º, 117.62º, 129.86º). All the tetrahedral angles of the DPF ring are nearly 0º or 180º, which represents its planar nature. The variety in bond angles depends on the electronegativity of the oxygen atom, the present of lone pair electrons and the coupling of the double bonds. In calculation, the effect of conjugation between the phenyl and furan ring can be understood from the rise in bond lengths of C2-Cl9 and C5-C8 (both 1.540Å by B3LYP and 1.5262 and 1.4978 Å by experimental).

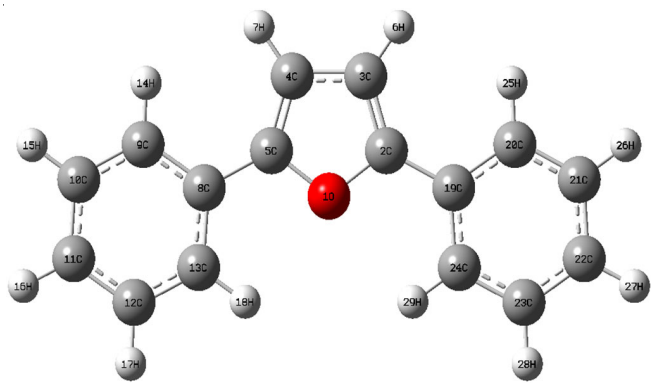

Fig. 1. Optimized structure of 2,5-diphenyl furan

The thermodynamic parameters of DPF are given in Table-2. As the interaction between the atoms within the molecule is very stronger, then the dipole moment will be extreme. Here,

TABLE-1
OPTIMIZED STRUCTURAL PARAMETERS OF 2,5-DIPHENYL FURAN
CALCULATED BY THE DFT/B3LYP METHOD WITH 6-311++G (d,p) BASIS SET

Bond length (Å)	B3LYP/6-311++G(d,p)	Exp. [23]	Bond angle (°)	B3LYP/6-311++G(d,p)	Exp. [23]	Dihedral angles (°)	B3LYP/6-311++G(d,p)	Exp. [23]
O1-C2	1.3955	1.3910	C2-O1-C5	106.56	107.52	C5-O1-C2-C3	-0.0117	-0.26
O1-C5	1.3953	1.3730	O1-C2-C3	110.08	107.08	C5-O1-C2-C19	179.9964	179.90
C2-C3	1.3796	1.3750	O1-C2-C19	114.45	117.62	C2-O1-C5-C4	0.0092	0.0072
C2-C19	1.5400	1.5262	C3-C2-C19	135.46	133.76	C2-O1-C5-C8	-179.994	-179.49
C3-C4	1.4480	1.4222	C2-C3-C4	106.64	107.96	O1-C2-C3-C4	0.0097	0.0020
C3-H6	1.0858	0.9300	C2-C3-H6	127.73	126.20	O1-C2-C3-C6	-179.997	-177.18
C4-C5	1.3797	1.3745	C4-C3-H6	125.62	129.12	C19-C2-C3-C4	179.9992	178.47
C4-H7	1.0857	0.9300	C3-C4-C5	106.58	107.02	C19-C2-C3-C6	-0.0078	-0.0031
C5-C8	1.5400	1.4978	C3-C4-H7	125.64	126.02	O1-C2-C19-C20	179.9839	178.47
C8-C9	1.3948	1.3662	C5-C4-H7	127.76	129.86	H6-C3-C4-C5	-179.997	-179.90
C8-C13	1.3952	1.3672	O1-C5-C4	110.12	110.30	H6-C3-C4-H7	0.0071	0.0011
C9-C10	1.3951	1.3810	O1-C5-C8	114.44	118.61	C3-C4-C5-O1	-0.0033	-0.0034
C9-H14	1.0996	0.9300	C4-C5-C8	135.43	138.27	C3-C4-C5-C8	-179.999	-179.78
C10-C11	1.3948	1.3725	C5-C8-C9	120.00	122.92	H7-C4-C5-O1	179.9924	179.56
C10-H15	1.0998	0.9300	C5-C8-C13	119.99	117.30	H7-C4-C5-C8	-0.0032	-0.0047
C11-C12	1.3954	1.3862	C9-C8-C13	119.99	118.61			
C11-H16	1.0997	0.9300	C8-C9-C10	120.00	119.29			
C12-C13	1.3947	1.3872	C8-C9-H14	120.00	120.18			
C12-H17	1.0997	0.9700	C10-C9-H14	119.99	119.90			
C13-H18	1.0997	0.9700	C9-C10-C11	120.00	119.90			
C19-C20	1.3948	1.3822	C9-C10-H15	119.98	120.62			
C19-C24	1.3952	1.3792	C11-C10-H15	120.01	119.70			
C20-C21	1.3951	1.3852	C10-C11-C12	119.99	120.20			
C20-H25	1.0996	0.9600	C10-C11-H16	120.02	120.02			
C21-C22	1.3948	1.3286	C12-C11-H16	119.98	120.30			
C21-H26	1.0998	0.9700	C11-C12-C13	119.99	119.80			
C22-C23	1.3954	1.4494	C11-C12-H17	119.99	119.80			
C22-H27	1.0997	0.9600	C13-C12-H17	120.01	120.64			
C23-C24	1.3947	1.3962	C8-C13-C12	120.00	119.70			
C23-H28	1.0997	0.9600	C8-C13-H18	119.98	119.70			
C24-H29	1.0997	0.9600	C12-C13-H18	120.01	122.92			
			C2-C19-C20	120.00	123.73			
			C2-C19-C24	119.99	116.47			
			C20-C19-C24	119.99	116.45			
			C19-C20-C21	120.00	119.73			
			C19-C20-H25	120.00	117.90			
			C21-C20-H25	119.99	116.78			
			C20-C21-C22	120.00	119.80			
			C20-C21-H26	119.98	119.80			
			C22-C21-H26	120.01	124.80			
			C21-C22-C23	119.99	120.20			
			C21-C22-H27	120.02	120.20			
			C23-C22-H27	119.98	119.71			
			C22-C23-C24	119.99	119.80			
			C22-C23-H28	119.99	119.80			
			C24-C23-H28	120.01	121.11			
			C19-C24-C23	120.00	118.50			
			C19-C24-H29	119.98	120.17			
			C23-C24-H29	120.01	122.89			

the calculated dipole moment and total energy of DPF were evaluated as 0.5991 Debye and 152.980 kcal mol^{-1}, respectively. The irrel-evant vibrational energy (zero-point) was obtained (144.83561 kcal mol^{-1}) for DPF. These thermodynamic parameters can be utilized in the assessment of chemical responses and to discover the extra thermodynamic energies for DPF.

Vibrational assignments: The computed and experimental FTIR and FT-Raman spectra of DPF have been represented in Figs. 2 and 3. The IR and Raman peak intensities and the vibrational wavenumbers of DPF are shown in Table-3. The DPF molecule comprises of 29 atoms and its leads to 81 typical vibrational modes.

C-H vibrations: The C-H vibrations are found within the range 3100-3000 cm^{-1} [25]. Subsequently, the infrared bands that showed up at 3142, 3139, 3133, 3097, 3094, 3092, 3088, 3084, 3077, 3054, 3042, 3027 cm^{-1} and in Raman spectra 3151,

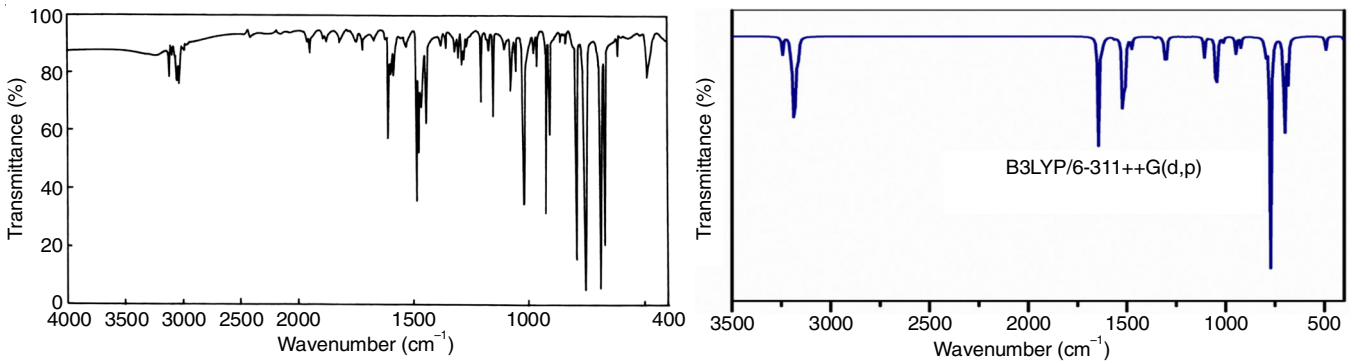

Fig. 2. FT-IR spectrum of 2,5-diphenyl furan

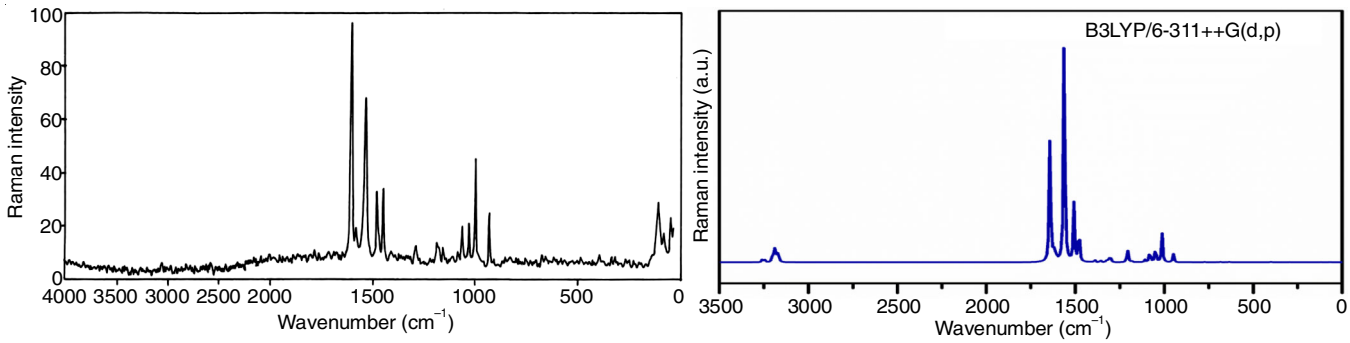

Fig. 3. FT-Raman spectrum of 2,5-diphenyl furan

TABLE-2
THERMODYNAMIC PARAMETERS OF 2,5-DIPHENYL FURAN

Parameters	B3LYP/6-311++G(d.p)
Optimized global minimum energy (Hartrees)	-692.3243481
Total energy (thermal), E_{total} (kcal mol^{-1})	152.980
Heat capacity, C_v (cal mol^{-1} k^{-1})	51.991
Entropy, S (cal mol^{-1} k^{-1})	117.549
Total	
Translational	42.070
Rotational	32.972
Vibrational	42.508
Vibrational energy, E_{vib} (kcal mol^{-1})	151.202
Zero point vibrational energy, (kcal mol^{-1})	144.83561
Rotational constants (GHz)	
A	1.43456
B	0.21694
C	0.18844
Dipole moment (Debye)	0.5991

3095, 3098, 3033 cm^{-1} for DPF have been assigned to C-H stretching vibrations. The DFT values at 3132, 3119, 3078, 3077, 3068, 3067, 3059, 3058, 3948, 3047, 3041, 3040 (nearly 99% TED) shows the good agreement with the experimental results. Both the computed and experimental C-H stretching vibrations have appeared great assertion with the literature data [26]. In Table-3, the C-H bending vibrations are also listed.

C-C and C-O Vibrations: In the heterocyclic compounds, the C-C vibrations built up in the range between 1430 and 1650 cm^{-1} [27]. In present examination, the C-C (nearly 90% TED) vibrations of DPF is observed at 1632, 1618, 1617, 1538, 1523, 1503, 1488, 1472, 1471, 1470, 1391, 1356, 1355, 1331, 1321, 1142, 1141, 1139 cm^{-1} in the FTIR and at 1648, 1620, 1544, 1525, 1509, 1487, 1478, 1381, 1361, 1132 cm^{-1} in FT-Raman spectrum. The corresponding computed peak are obtained at 1581, 1578, 1563, 1554, 1543, 1502, 1462, 1450, 1423, 1418, 1336, 1306, 1305, 1276, 1268, 1180, 1159, 1156 and 1137 cm^{-1}. The C-C in-plane vibrations are found at 812 and 777 cm^{-1} in IR and the corresponding DFT frequencies at 812 and 768 cm^{-1}. The out of plane C-C modes of vibrations for DPF are also given in Table-3. The C-O stretching (nearly 79% TED) modes of DPF are joined with other vibrational modes [28], which were observed experimentally at 1298, 1248 and 1257 cm^{-1}. The calculated C-O vibrational modes were found at 1254 and 1241 cm^{-1}.

Frontier molecular orbital (FMO) analysis: The stabilization and destabilization of the molecule can increase because of the HOMO and LUMO orbitals [29]. The HOMO-LUMO of DPF has been computed at the DFT levels and energy gap is found to be 2.7113 eV, which reflects the chemical activity of DPF and are illustrated in Table-4. The most notable (E_{HOMO} = -8.3223 eV) HOMO energy permits to be the excellent electron giver (phenyl and furan) and the LUMO (E_{LUMO}= -5.6109 eV) implies the leading electron acceptor (C-C bond of ring). The corresponding energy gap of DPF is plotted in Fig. 4. Further, the frequency of oscillation (f), excitation energies (E), electronic transition and UV-vis spectral studies of DPF were computed by TD-DFT method [30,31]. The energizing state of DPF was found at 342.33 nm with energy E = 3.6218 eV and oscillator frequency of 0.8422. For this strong peak, the transition of charges from HOMO to LUMO describes $\pi \rightarrow \pi^*$ (99% contribution) as exposed in Fig. 5. Another energize state from H→L+1 ($\pi \rightarrow \pi^*$ type) has been computed at 292.91 nm with frequency f = 0.0037, E = 4.2329 eV leading to the contribution

TABLE-3
CALCULATED VIBRATIONAL FREQUENCIES (cm^{-1}), IR INTENSITIES (Km mol^{-1}), RAMAN SCATTERING ACTIVITY ($Å^4$ amu^{-1}), REDUCED MASS (amu), FORCE CONSTANTS (mDyne/$Å^{-1}$) AND VIBRATIONAL ASSIGNMENTS BASED ON PED CALCULATIONS FOR 2,5-DIPHENYL FURAN

Observed wavenumber		Wavenumber (cm^{-1})		IR Intensity	Raman activity	Reduced mass	Force constant	Assignment with PED (%)
FT-IR	FT-Raman	Calculated	Scaled					
3142(ms)	3151(ms)	3258	3132	0.2894	108.0479	1.1010	6.8855	νC-H (99)
3139(vw)	–	3245	3119	10.2338	76.1738	1.0927	6.7788	νC-H (98)
3133(vw)	–	3202	3078	8.0120	176.7709	1.0936	6.6056	νC-H (97)
3097(vw)	3095(ms)	3201	3077	0.1715	4.5720	1.0937	6.6047	νC-H (97)
3094(ms)	–	3191	3068	1.7302	519.2148	1.0963	6.5750	νC-H (96)
3092(vw)	–	3190	3067	40.3070	9.5296	1.0963	6.5744	νC-H (94)
3088(vw)	–	3182	3059	34.8555	27.8866	1.0922	6.5155	νC-H (90)
3084(vw)	3098(ms)	3181	3058	4.1987	135.7530	1.0922	6.5152	νC-H (92)
3077(ms)	–	3171	3048	6.2567	201.7226	1.0884	6.4470	νC-H (92)
3054(ms)	–	3170	3047	3.5974	58.4112	1.0883	6.4465	νC-H (91)
3042(ms)	3033(ms)	3163	3041	1.2931	28.3592	1.0852	6.3968	νC-H (91)
3027(ms)	–	3162	3040	6.9898	46.7920	1.0852	6.3963	νC-H (90)
1632(ms)	1648(ms)	1645	1581	58.4660	601.7473	5.6354	8.9810	νC-C (89)
1618(ms)	1620(vs)	1642	1578	3.4229	2583.6280	5.4303	8.6248	νC-C (90)
1617(ms)	–	1626	1563	6.2194	46.2159	6.2520	9.7395	νC-C (87)
1538(vs)	1544(vs)	1617	1554	1.8910	303.0112	5.6300	8.6722	νC-C (88)
1523(vs)	1525(vs)	1605	1543	0.4199	48.1359	5.0989	7.7362	νC-C (87)
1503(vs)	1509(vs)	1562	1502	1.2579	5473.7882	4.9850	7.1675	νC-C (86)
1488(vs)	1487(vs)	1521	1462	63.5391	0.3372	2.2079	3.0084	νC-C (88)
1472(vs)	1478(vs)	1508	1450	21.7768	1220.1738	2.5488	3.4147	νC-C (85)
1471(vs)	–	1480	1423	1.7124	828.5698	2.4337	3.1398	νC-C (84)
1470(ms)	–	1475	1418	5.5466	1.8788	2.2317	2.8607	νC-C (82)
1391(ms)	1381(ms)	1390	1336	0.0673	52.5506	2.8733	3.2707	νC-C (81)
1356(ms)	1361(ms)	1359	1306	0.2383	0.8210	1.5977	1.7373	νC-C (83)
1355(ms)	–	1358	1305	0.8651	39.9953	1.8229	1.9812	νC-C (80)
1331(ms)	–	1327	1276	0.1209	26.0379	4.0999	4.2532	νC-C (82)
1321(ms)	–	1319	1268	1.4515	39.0200	4.3362	4.4414	νC-C (81)
1298(ms)	–	1304	1254	25.0950	163.7096	3.0855	3.0912	νC-O (79)
1248(ms)	1257(ms)	1291	1241	0.1618	4.2233	3.9517	3.8797	νC-O (78)
1142(ms)	–	1228	1180	0.1142	0.2574	1.8953	1.6847	νC-C (80)
1141(ms)	–	1206	1159	0.2987	285.4532	1.1413	0.9785	νC-C (81)
1139(ms)	–	1203	1156	0.0848	12.2670	1.1898	1.0144	νC-C (79)
1138(ms)	1132(s)	1183	1137	0.1575	12.7882	1.1087	0.9141	νC-C (80)
1124(s)	1128(s)	1182	1136	0.1018	12.8042	1.1089	0.9139	bCH (76)
1121(s)	–	1109	1066	11.3665	50.4855	1.7862	1.2932	bCH (74)
1111(s)	–	1104	1061	0.7848	0.0122	1.6829	1.2076	bCH (75)
1048(s)	1046(s)	1086	1044	0.0172	2.5794	2.4300	1.6898	bCH (74)
1019(s)	1028(s)	1080	1038	1.0912	249.2943	2.5240	1.7361	bCH (75)
1010(ms)	1005(ms)	1049	1008	29.8365	310.2104	1.4169	0.9183	bCH (72)
1007(ms)	–	1046	1006	11.0728	0.2728	2.5648	1.6539	bCH (73)
987(ms)	–	1044	1004	4.3490	4.9908	2.9049	1.8646	bCH (74)
982(ms)	991(ms)	1013	974	2.5666	19.5300	6.1711	3.7331	bCH (74)
967(ms)	996(ms)	1012	973	0.6353	530.2856	5.9959	3.6215	bCH (75)
965(ms)	–	997	958	0.0420	0.1715	1.2834	0.7505	bCH (73)
963(ms)	–	996	957	0.0001	2.0364	1.2857	0.7517	bCH (72)
953(s)	–	981	943	0.0077	0.0073	1.3598	0.7710	R1trigd (70)
929(vs)	921(ms)	980	942	0.0000	0.0101	1.3624	0.7721	R1asymd (69)
914(vs)	–	949	912	9.7974	160.3276	7.0093	3.7174	R1symd (68)
912(vs)	–	936	899	0.0018	0.2258	6.5319	3.3698	R2trigd (71)
911(vs)	–	924	888	6.0750	0.0343	1.4386	0.7230	R2asymd (68)
909(vs)	–	922	886	0.0000	0.0672	1.4399	0.7207	R3asymd (67)
832(vs)	841(vs)	864	831	0.0000	5.2754	1.3858	0.6094	R3symd (68)
817(s)	826(s)	850	817	0.1926	0.1092	1.2547	0.5337	R3trigd (69)
812(s)	–	845	812	0.0000	0.8170	1.2958	0.5449	bC-C (73)
777(s)	–	799	768	11.6575	1.1389	1.5929	0.5987	bC-C (73)
754(s)	–	774	744	0.0005	6.8744	1.8938	0.6671	bCO (71)

724(s)	729(s)	773	743	135.1931	0.1877	1.5490	0.5454	bCO (70)
713(vs)	–	708	681	13.4088	2.2191	6.2887	1.8586	ωCH (68)
632(vs)	–	701	674	51.8886	0.0404	1.9568	0.5667	ωCH (66)
643(vs)	–	700	673	0.0007	0.0036	1.8273	0.5287	ωCH (65)
657(vs)	661(vs)	686	659	3.1807	9.9233	6.5596	1.8171	ωCH (67)
645(ms)	–	684	656	21.1149	0.0977	3.7954	1.0472	ωCH (65)
634(ms)	645(ms)	654	629	0.0000	2.0531	3.0753	0.7756	ωCH (64)
624(ms)	625(ms)	633	609	0.0141	4.4649	6.4256	1.5186	ωCH (66)
616(ms)	607(ms)	632	608	0.0597	5.4111	6.4328	1.5178	ωCH (65)
526(s)	511(s)	522	502	0.0213	0.8836	5.1097	0.8196	ωCH (64)
514(vw)	498(vw)	505	485	0.0000	0.4716	3.2822	0.4928	ωCH (62)
512(w)	–	494	475	8.9721	0.0000	3.4857	0.5008	ωCH (65)
448(w)	437(w)	410	394	0.0000	0.0034	2.8918	0.2852	ωCH (64)
447(vw)	–	409	393	0.0015	0.0179	2.9033	0.2863	ωC-C (65)
441(w)	–	402	386	2.0032	1.4624	6.0194	0.5727	ωC-C (64)
400(w)	392(vw)	400	384	0.4380	8.6863	5.8510	0.5507	tR1trigd (61)
328(ms)	–	293	282	0.0000	3.1154	4.4171	0.2241	tR1asymd (63)
314(ms)	–	261	251	0.1245	0.6974	6.0436	0.2428	tR1symd (60)
303(ms)	221(ms)	238	229	0.1527	0.5218	5.3736	0.1791	tR2trigd (61)
142(ms)	–	180	173	0.8773	0.4484	4.6014	0.0878	tR2asymd (62)
118(ms)	–	119	114	0.0000	2.6417	4.8959	0.0406	ωCO (61)
92(ms)	–	83	80	3.0442	0.0148	4.9399	0.0199	ωCO (62)
56(ms)	–	70	67	0.0584	6.1433	5.0989	0.0145	tR3symd (61)
42(ms)	–	32	31	0.0007	0.8105	4.0647	0.0025	tR3trigd (60)
28(ms)	–	17	16	0.0000	1.0342	3.6053	0.0007	tR3asymd (59)

TABLE-4
GLOBAL REACTIVITY DESCRIPTORS
FOR 2,5-DIPHENYL FURAN

Molecular properties	B3LYP/6-311++G(d,p)
HOMO (eV)	-8.3223
LUMO (eV)	-5.6109
ΔE (E_{HOMO}-E_{LUMO}) (eV)	2.7113
Ionization potential (I) (eV)	8.3223
Electron affinity (A) (eV)	5.6109
Global hardness (η) (eV)	1.3557
Global softness (s) (eV^{-1})	0.3688
Electronegativity (χ) (eV)	6.9666
Chemical potential (μ) (eV)	-6.9666
Global electrophilicity (w) (eV)	17.9023

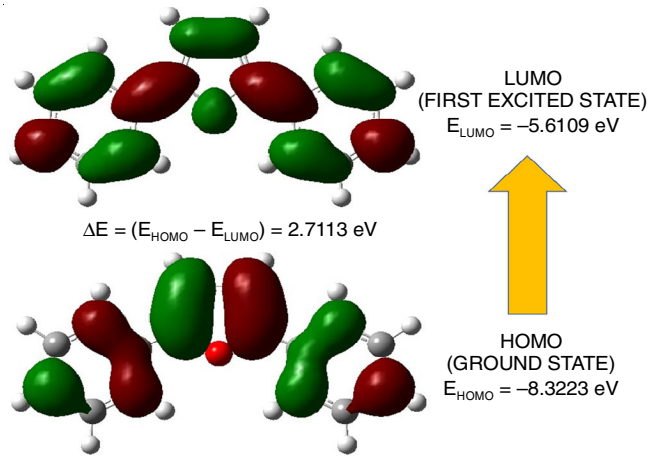

Fig. 4. HOMO-LUMO plot of 2,5-diphenyl furan

of 78% as listed in Table-5. Hence, the DPF has been unsaturated due to the π→π* type transition and reflects the Eigen values of HOMO and LUMO.

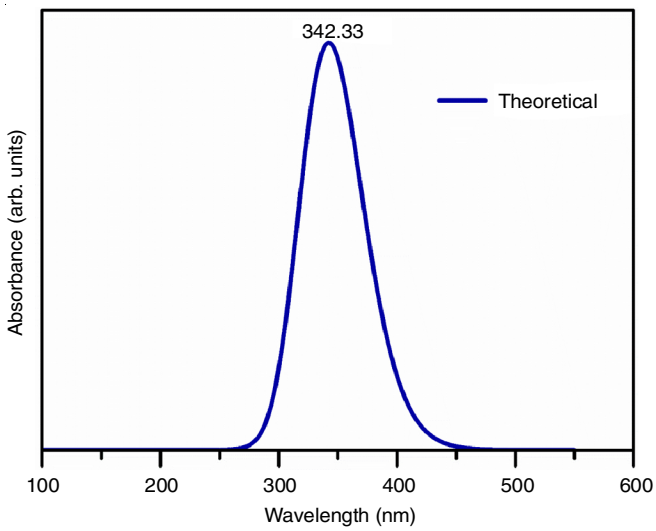

Fig. 5. UV plot of 2,5-diphenyl furan

TABLE-5
MOLECULAR ORBITAL CONTRIBUTIONS
OF 2,5-DIPHENYL FURAN

TDDFT/B3LYP/6-311++G(d,p) method				
Energy (eV)	Oscillator strength	Wavelength (nm)	Major contributions	Assignment
3.6218	0.8422	342.33	H→L (99%)	π–π*
4.2329	0.0037	292.91	H→L+1(78%)	π–π*

Mulliken atomic charges: The reactive charges show the dynamic applications in the quantum chemical calculation, since they affect the electronic properties of the molecule [32]. Also, the Mullikan charge has been utilized to explain the forms of electronegativity balance and exchange in chemical responses to exterior molecular surfaces. The Mulliken plot utilizing

B3LYP with 6-311++G (d,p) basis set for DPF is given in Fig. 6 and values are recorded in Table-6. The positive values (0.159078, 0.159079, 0.084600, 0.181892, 0.145477, 0.182620, 0.106298, 0.084602, 0.181892, 0.145477, 0.182620 and 0.106296) of H6, H7, H14, H15, H16, H17, H18, H25, H26, H28 and H29 represents that DPF is more acidic. The partial charges on C2 and C5 are highly influenced by their substituents. Further, the C23 and C12 dominate the largest negative charge for DPF (-0.215537 and -0.215536).

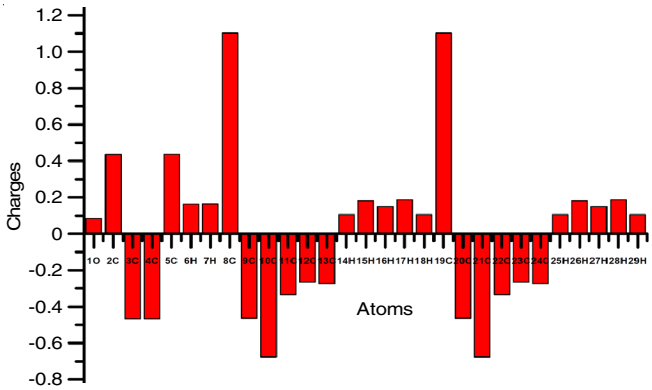

Fig. 6. Mulliken charges plot for 2,5-diphenyl furan

TABLE-6
MULLIKEN ATOMIC CHARGE FOR 2,5-DIPHENYL FURAN

Atom	B3LYP/6-311++G(d.p)	Atom	B3LYP/6-311++G(d.p)
O1	0.049028	H16	0.145477
C2	0.601996	H17	0.182620
C3	-0.434261	H18	0.106298
C4	-0.434263	C19	1.106332
C5	0.601888	C20	-0.636557
H6	0.159078	C21	-0.675757
H7	0.159079	C22	-0.385071
C8	1.106319	C23	-0.215537
C9	-0.636572	C24	-0.245507
C10	-0.675758	H25	0.084602
C11	-0.385074	H26	0.181892
C12	-0.215336	H27	0.145477
C13	-0.24490	H28	0.182620
H14	0.084600	H29	0.106296
H15	0.181892	–	–

NMR spectral analysis: GIAO strategy is used to obtain the ^{13}C and ^{1}H NMR spectra for DPF using DFT/B3LYP 6-311++G (d,p). It is one of the efficient methods to simulate the structure of larger biomolecules [33]. The computational ^{13}C and ^{1}H isotropic shift values of DPF with tetramethyl silane (TMS) as a reference is recorded on Table-7 and expressed in Fig. 7. In general, the aromatic carbon shows chemical shift in the range from 100 to 200 ppm [34]. In this study, the chemical shifts of aromatic carbons were obtained from 111.34 ppm and 159.80 ppm. Due to the high electronegativity of oxygen atom (O1), the higher shifts were obtained for C2 and C5 (both 159.80 ppm). The lower shift obtained at 111.34 ppm for C4 is due to the fact that it was coupled with H atom. In ^{1}H NMR, the lowest shifts were obtained at 6.78 ppm due to the H6 and H7 protons as shown in Fig. 7. The chemical shifts of H14, H17, H18, H25 and H29 were directly attached with carbon atoms so that they have extreme shift of 7.78, 7.50, 8.19, 7.78 and 8.19 ppm.

TABLE-7
^{13}C AND ^{1}H NMR CHEMICAL SHIFTS FOR 2,5-DIPHENYL FURAN

^{13}C assignment	Calculated Shift (ppm)	^{1}H assignment	Calculated shift (ppm)
C2	159.80	H18	8.19
C5	159.80	H29	8.19
C19	136.32	H14	7.78
C8	136.32	H25	7.78
C12	133.88	H17	7.50
C23	133.88	H28	7.50
C10	133.30	H15	7.39
C21	133.30	H26	7.39
C11	131.12	H16	7.27
C22	131.12	H27	7.27
C20	127.53	H7	6.78
C9	127.53	H6	6.78
C13	127.30	–	–
C24	127.30	–	–
C3	111.34	–	–
C4	111.34	–	–

Molecular electrostatic potential surface analysis: The MEP surface of DPF molecule is shown in Fig. 8. Blue and red represents the region of most attractive and repulsive

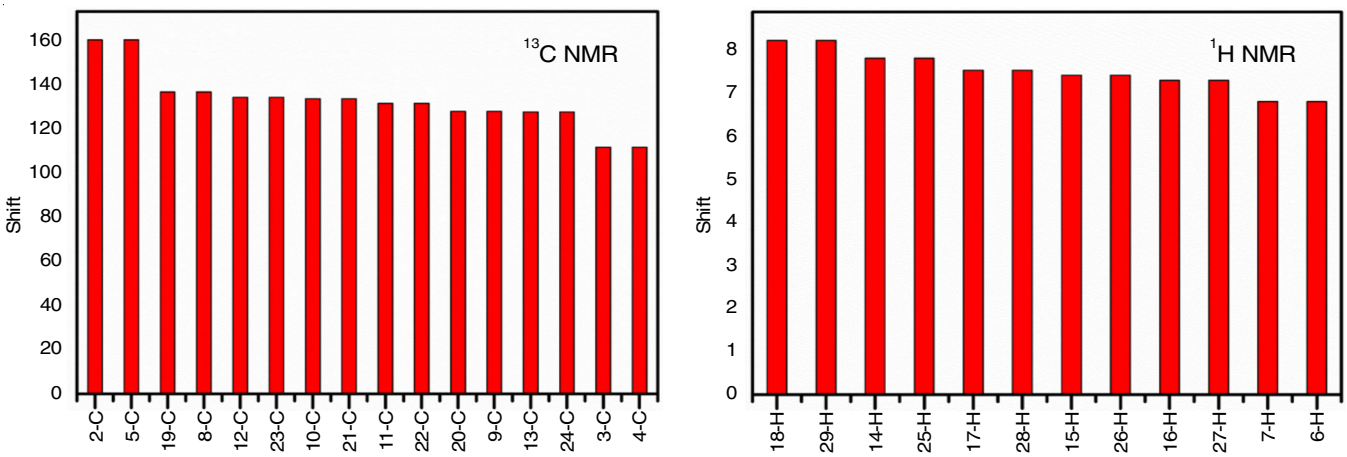

Fig. 7. ^{13}C and ^{1}H NMR theoretical spectra for 2,5-diphenyl furan

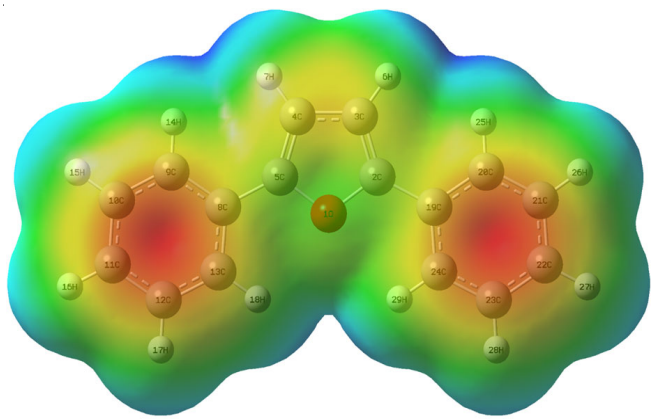

Fig. 8. MEP plot of 2,5-diphenyl furan

regions, respectively [35]. In DPF, the negative potential was found over the oxygen atom (O1), due to lone pair of negative charges. The positive locales are nucleophilic and are found on the hydrogens of phenyl group and hydrogens (H7 and H6) attached with the furan ring. The MEP of DPF explains that the phenyl and furan rings are probable outbreak for the reactive sites.

Natural bonding orbital analysis (NBO): In DPF, the NBO investigation was executed using B3LYP/6-311++G(d,p) basis set and the obtained results are recorded in Table-8. In general, greater the stabilization energy, that will be more tendency to donate(i) electrons to acceptor(j) orbitals [36]. The ICT interaction from the σ to σ* orbitals is the distinctive feature for medicinal compound [37]. In DPF, the solid intra-molecular interaction energy is gotten between the σ (C19-C24) and σ* (C4-C5) orbital, which cause the maximum stabili-zation energy of 16251.67 kcal mol^{-1}. Furthermore, the significant σ to σ* charge exchanges lead to the optimistic polarization and that gives more biological activity to DPF.

Molecular docking: In this work, the DPF molecule was taken as a ligand and SARS-CoV-2 M^{pro} [PDB ID: 7JMO] is used as focused protein. From the previous report, this protein expression helps to reduce the development of SARS-CoV-2 M^{pro} [38]. Fig. 9 shows the 3D representation of docked ligand (DPF) at the binding site of the targeted protein SARS-CoV-2 M^{pro}. In addition, the corresponding calculated binding energy values are given in Table-9a. The obtained docking outcomes revealed that the interaction between DPF and SARS-CoV-2 M^{pro} makes hydrophobic interaction with the restraint consistent energies, intermolecular vitality and amino acid residues GLNC:923, ASNC:714, LEU:919, SER:144, CYS:145, HIS:41, GLU:166 (Table-9b). The free binding energy (ΔG°) for SARS-CoV-2 M^{pro} was found to be −8.01 $KJmol^{-1}$. These outcomes will be useful in the development of workable drugs for the treatment of SARS-CoV-2 M^{pro} disease. Hence, it is sensible

TABLE-8
SECOND-ORDER PERTURBATION THEORY ANALYSIS OF FOCK MATRIX FOR 2,5-DIPHENYL FURAN MOLECULE BY NBO ANALYSIS

Donor(i)	ED(i) (e)	Acceptor (j)	ED (j) (e)	Stabilization energy E(2) (kJ mol^{-1})	Energy difference E(j) – E(i) (a.u.)	Fock matrix element F (I,j) (a.u.)
σ(C2-C19)	1.97377	σ*(C23-H28)	0.01371	543.51	0.02	0.093
σ(C5-C8)	1.97377	σ*(C23-H28)	0.01371	4726.48	0.33	1.115
σ(C8-C9)	1.96736	σ*(C23-H28)	0.01371	3662.76	0.12	0.6
σ(C19-C20)	1.96736	σ*(C4-C5)	0.01986	3191.94	29.58	8.702
σ(C19-C20)	1.96736	σ*(C19-C24)	0.02416	7933.55	26.65	13.006
σ(C19-C20)	1.96736	π*(C19-C24)	0.38711	13437.78	22.07	16.948
σ(C19-C20)	1.96736	σ*(C20-C21)	0.01527	12193.8	23.35	15.129
σ(C19-C20)	1.96736	σ*(C23-C24)	0.01550	12676.59	25.1	15.992
σ(C19-C20)	1.96736	σ*(C23-H28)	0.01371	3477.81	31.01	9.315
σ(C19-C24)	1.96838	σ*(C4-C5)	0.01986	16251.67	0.4	2.286
σ(C19-C24)	1.96838	σ*(C23-H28)	0.01371	2973.75	1.83	2.094
σ(C20-C21)	1.97664	σ*(C23-H28)	0.01371	3327.84	0.08	0.473
π(C20-C21)	1.68398	σ*(C4-C5)	0.01986	5057.48	2.36	3.34
σ(C22-C23)	1.97969	σ*(C4-C5)	0.01986	3527.42	27.6	8.809
σ(C22-C23)	1.97969	σ*(C19-C24)	0.02416	7607.54	24.67	12.24
σ(C22-C23)	1.97969	π*(C19-C24)	0.38711	13832.23	20.09	16.467
σ(C22-C23)	1.97969	σ*(C20-C21)	0.01527	15143.64	21.37	16.08
σ(C22-C23)	1.97969	σ*(C23-C24)	0.01550	6264.55	23.12	10.756
σ(C22-C23)	1.97969	σ*(C23-H28)	0.01371	1511.33	29.04	5.923
π(C22-C23)	1.65867	σ*(C4-C5)	0.01986	5056.04	2.3	3.324
π(C22-C23)	1.65867	σ*(C23-H28)	0.01371	1774.23	3.73	2.513
σ(C23-C24)	1.97704	σ*(C23-H28)	0.01371	12401.74	0.04	0.6
π*(C19-C24)	0.38711	σ*(C19-C24)	0.02416	2988.67	4.58	7.28
π*(C19-C24)	0.38711	σ*(C20-C21)	0.01527	15926.28	1.28	8.996
π*(C19-C24)	0.38711	σ*(C23-C24)	0.01550	4843.42	3.03	7.623
π*(C22-C23)	0.33825	σ*(C19-C24)	0.02416	1278.13	394.2	47.069
π*(C22-C23)	0.33825	π*(C19-C24)	0.38711	4478.19	389.62	61.913
π*(C22-C23)	0.33825	σ*(C23-C24)	0.01550	1494.84	392.65	51.421

TABLE-9a
MOLECULAR DOCKING RESULTS FOR 2,5-DIPHENYL FURAN WITH SARS-COV-2 M^{pro}

Protein	Binding energy	Ligand efficiency	Inhibit constant	Intermol energy	vdw HB dissolve energy	Electrostatic energy	Total internal	Torsional energy	Unbound energy
(SARS-CoV-2 M^{pro}) (PDB ID: 7JMO)	-8.10	-0.66	37.34	-8.54	-8.26	-0.03	-0.04	0.8	-0.03

TABLE-9b
DOCKING CALCULATION SHOWING INTERACTIVE RESIDUES, BINDING RESIDUES INVOLVED IN H-BONDING TO ACTIVE SITES

Protein	Interacted Residues	Ligand and protein atom involved in H-bonding
(SARS-CoV-2 M^{pro}) (PDB ID: 7JMO)	GLNC:923, ASNC:714, LEU:919, SER:144; CYS:145, HIS41, GLU166	SER:144

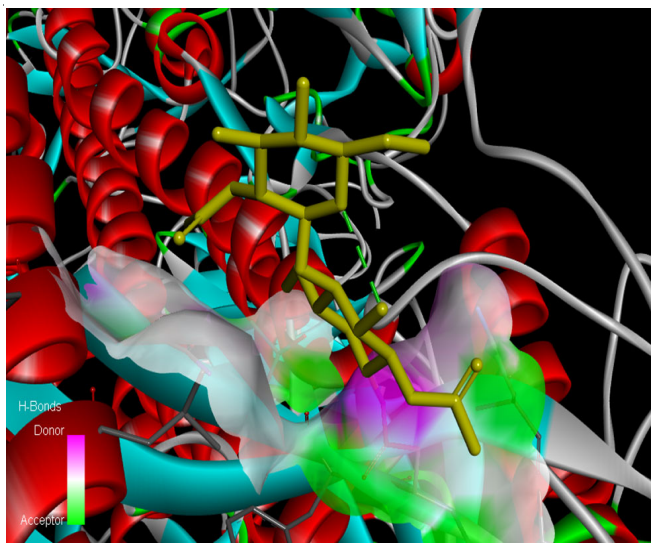

Fig. 9. 2,5-Diphenyl furan interacts with the (SARS-CoV-2 Mpro) (PDB ID: 7JMO) protein marker

to speculate that the DPF might have powerful SARS-CoV-2 M^{pro} action.

Conclusion

This study focused towards the development of potential inhibitors for the SARS-CoV-2 M^{pro} with the help of advanced computational approach. The optimized structural parameters and spectroscopic studies of 2,5-diphenyl furan was investigated by using DFT method. The frequencies of all the normal modes were analyzed and found to be in good agreement with the DFT results. The MEP analysis provides the electrophilic and nucleophilic responses of the molecule. The chemical activity of 2,5-diphenyl furan molecule was ensured by the Mulliken charge distribution and FMOs analysis. The ^{13}C and ^{1}H NMR studies reflect the structural information of the molecule. The intra and intermolecular charge exchange have been understood from the NBO studies. These results indicates that the 2,5-diphenyl furan will be a potential material in the treatment of SARS-CoV-2 M^{pro} action.

CONFLICT OF INTEREST

The authors declare that there is no conflict of interests regarding the publication of this article.

REFERENCES

1. G. Derosa, P. Maffioli, A. D'Angelo and F. Di Pierro, *Phytother. Res.*, **35**, 1230 (2021); https://doi.org/10.1002/ptr.6887
2. S.T. Ngo, N. Quynh Anh Pham, L. Thi Le, D.-H. Pham and V.V. Vu, *J. Chem. Inf. Model.*, **60**, 5771 (2020); https://doi.org/10.1021/acs.jcim.0c00491
3. G.R. Marshall, *Annu. Rev. Pharmacol. Toxicol.*, **27**, 193 (1987); https://doi.org/10.1146/annurev.pa.27.040187.001205
4. M. Rani, M. Yusuf, S.A. Khan, P.P. Sahota and G. Pandove, *Arab. J. Chem.*, **8**, 174 (2015); https://doi.org/10.1016/j.arabjc.2010.10.036
5. M. Rani, M. Yusuf and S.A. Khan, *J. Saudi Chem. Soc.*, **16**, 431 (2012); https://doi.org/10.1016/j.jscs.2011.02.012
6. J.-Q. Huo, L.-Y. Ma, Z. Zhang, Z.-J. Fan, J.-L. Zhang, T.V. Beryozkina and V.A. Bakulev, *Chin. Chem. Lett.*, **27**, 1547 (2016); https://doi.org/10.1016/j.cclet.2016.06.019
7. L.A. Anthony, D. Rajaraman, M. Shanmugam and K. Krishnasamy, *Chem. Data Coll.*, **28**, 100421 (2020); https://doi.org/10.1016/j.cdc.2020.100421
8. M.R. Barros, T.M. Menezes, L.P. Da Silva, D.S. Pires, J.L. Princival, G. Seabra and J.L. Neves, *Int. J. Biol. Macromol.*, **136**, 1034 (2019); https://doi.org/10.1016/j.ijbiomac.2019.06.120
9. K. Srikanth Kumar, A. Lakshmana Rao and D.R. Sekhara Reddy, *Indian J. Pharm. Educ. Res.*, **55**, 266 (2021); https://doi.org/10.5530/ijper.55.1.30
10. M.E., Vaschetto, B.A. Retamal and A.P. Monkman, *J. Mol. Struct. Theochem.*, **468**, 209 (1999); https://doi.org/10.1016/S0166-1280(98)00624-1
11. S. Premkumar, A. Jawahar, T. Mathavan, M.K. Dhas, V.G. Sathe and A.M.F. Benial, *Spectrochim. Acta A Mol. Biomol. Spectrosc.*, **129**, 74 (2014); https://doi.org/10.1016/j.saa.2014.02.147
12. T. Lengauer and M. Rarey, *Curr. Opin. Struct. Biol.*, **6**, 402 (1996); https://doi.org/10.1016/S0959-440X(96)80061-3
13. M.J. Frisch, G.W. Trucks, H.B. Schlegal, G.E. Scuseria, M.A. Robb, J.R. Cheesman, V.G. Zakrzewski, J.A. Montgomerg Jr., R.E. Stratmann, J.C. Burant, S. Dapprich, J.M. Millam, A.D. Daniels, K.N. Kudin, M.C. Strain, O. Farkas, J. Tomasi, V. Barone, M. Cossi, R. Cammi, B. Mennucci, C. Pomelli, C. Adamo, S. Clifford, J. Ochterski, G.A. Petersson, P.Y. Ayala, Q. Cui, K. Morokuma, N. Rega, P. Salvador, J.J. Dannenberg, D.K. Malich, A.D. Rabuck, K. Raghavachari, J.B. Foresman, J. Cioslowski, J.V. Ortiz, A.G. Baboul, B.B. Stetanov, G. Liu, A. Liashenko, P. Piskorz, I. Komaromi, R. Gomperts, R.L. Martin, D.J. Fox, T. Keith, M.A. Al-Laham, C.Y. Peng, A. Nanayakkara, M. Challacombe, P.M.W. Gill, B. Johnson, W. Chen, M.W. Wong, J.L. Andres, C. Gonzalez, M. Head-Gordon, E.S. Replogle and J.A. Pople, GAUSSIAN 09, Revision A 11.4, Gaussian, Inc, Pittsburgh. PA. (2009).
14. A.D. Becke, *J. Chem. Phys.*, **98**, 5648 (1993); https://doi.org/10.1063/1.464913
15. C. Lee, W. Yang and R.G. Parr, *Phys. Rev.*, **37**, 785 (1988); https://doi.org/10.1103/PhysRevB.37.785

16. M. Castellà-Ventura, E. Kassab, G. Buntinx and O. Poizat, *Physiol. Chem. Phys.*, **2**, 4682 (2000); https://doi.org/10.1039/b006459i
17. D.C. Young, Computational Chemistry: A Practical Guide for Applying Techniques to Real World Problems (Electronic) John Wiley & Sons Ltd.: New York (2001).
18. T. Keith and J. Milam, Gauss View, Version 5, Semichem Inc.; Shawnee Mission KS, Ray Dennington (2009).
19. MOLVIB (V.7.0), Calculation of Harmonic Force Fields and Vibrational Modes of Molecules, QCPE Program No. 807 (2002).
20. O. Trott and A.J. Olson, *J. Comput. Chem.*, **31**, 455 (2009); https://doi.org/10.1002/jcc.21334
21. U.P. Mohan, S. Kunjiappan, P.B. Tirupathi Pichiah and S. Arunachalam, *3 Biotech.*, **11**, 15 (2021); https://doi.org/10.1007/s13205-020-02530-9
22. B.L. Narayana, D. Pran Kishore, C. Balakumar, K.V. Rao, R. Kaur, A.R. Rao, J. Murthy and M. Ravikumar, *Chem. Biol. Drug Des.*, **79**, 674 (2012); https://doi.org/10.1111/j.1747-0285.2011.01277.x
23. X.G. Meng and A. Wu, *Acta Crystallogr. Sect. E Struct. Rep. Online*, **61**, o2808 (2005); https://doi.org/10.1107/S1600536805024554
24. M.K. Ahmed and B.R. Henry, *J. Phys. Chem.*, **90**, 1737 (1986); https://doi.org/10.1021/j100400a002
25. V. Siva, S.S. Kumar, M. Suresh, M. Raja, S. Athimoolam and S.A. Bahadur, *J. Mol. Struct.*, **1133**, 163 (2017); https://doi.org/10.1016/j.molstruc.2016.11.088
26. V. Siva, S.S. Kumar, A. Shameem, M. Raja, S. Athimoolam and S.A. Bahadur, *J. Mater. Sci. Mater. Electron.*, **28**, 12484 (2017); https://doi.org/10.1007/s10854-017-7070-8
27. G. Sivaraj, N. Jayamani and V. Siva, *J. Mol. Struct.*, **1240**, 130530 (2021); https://doi.org/10.1016/j.molstruc.2021.130530
28. M. Arivazhagan, S. Jeyavijayan and J. Geethapriya, *Spectrochim. Acta A Mol. Bio. Mol. Spectrosc.*, **104**, 14 (2013); https://doi.org/10.1016/j.saa.2012.11.032
29. S. Jeyavijayan, M. Ramuthai and P. Murugan, *Asian J. Chem.*, **33**, 2313 (2021); https://doi.org/10.14233/ajchem.2021.23308
30. S. Jeyavijayan and P. Murugan, *Asian J. Chem.*, **33**, 83 (2020); https://doi.org/10.14233/ajchem.2021.22922
31. N. Sundaraganesan, G. Elango, C. Meganathan, B. Karthikeyan and M. Kurt, *Mol. Simul.*, **35**, 705 (2009); https://doi.org/10.1080/08927020902873992
32. B. Pramodh, P. Naresh, S. Naveen, N.K. Lokanath, S. Ganguly, J. Panda, S. Murugesan, A.V. Raghu and I. Warad, *Chem. Data Coll.*, **31**, 100587 (2021); https://doi.org/10.1016/j.cdc.2020.100587
33. K. Rastogi, M.A. Palafox, R.P. Tanwar and L. Mittal, *Spectrochim. Acta A Mol. Biomol. Spectrosc.*, **58**, 1987 (2002); https://doi.org/10.1016/S1386-1425(01)00650-3
34. J. Luque, J.M. Lopez and M. Orozco, *Theor. Chem. Acc.*, **103**, 343 (2000); https://doi.org/10.1007/s002149900013
35. O. Noureddine, N. Issaoui and O. Al-Dossary, *J. King Saud Univ. Sci.*, **33**, 101248 (2021); https://doi.org/10.1016/j.jksus.2020.101248
36. M. Nsangou, Z. Dhaouadi, N. Jaïdane and Z. Ben Lakhdar, *J. Mol. Struct. THEOCHEM*, **819**, 142 (2007); https://doi.org/10.1016/j.theochem.2007.05.038
37. S.P. Vijaya Chamundeeswari, E. James Jebaseelan Samuel and N. Sundaraganesan, *Mol. Simul.*, **38**, 987 (2012); https://doi.org/10.1080/08927022.2012.682279
38. N.C. Wu, M. Yuan, H. Liu, C.-C.D. Lee, X. Zhu, S. Bangaru, J.L. Torres, T.G. Caniels, P.J.M. Brouwer, M.J. van Gils, R.W. Sanders, A.B. Ward and I.A. Wilson, *Cell Rep.*, **33**, 108274 (2020); https://doi.org/10.1016/j.celrep.2020.108274